Costs and Benefits of a Pearl River Delta Emission Control Area

Detailed methodology

By:
Xiaoli Mao
Chen Chen
Bryan Comer, Ph.D.
Dan Rutherford, Ph.D.

July 2019

THE INTERNATIONAL COUNCIL
ON CLEAN TRANSPORTATION

Acknowledgments

The authors thank members of the International Association for Catalytic Control of Ship Emissions to Air and Dr. Chuansheng Peng for the critical reviews and thoughtful recommendations, and our colleagues Josh Miller, Jennifer Callahan, and Hongyang Cui for their tremendous support in review and proofreading. We especially thank the Health Effects Institute for its generous support in providing mortality data. We also acknowledge Tsinghua University for providing gridded emissions inventory data for land-based sources in China for 2015 and 2030. This study was funded by Energy Foundation China with support from Bloomberg Philanthropies.

For additional information:

International Council on Clean Transportation

1500 K Street NW, Suite 650

Washington DC 20005 USA

Table of Contents

Tables

Figures

1. Introduction

This supporting document provides a detailed explanation of the methodology used by Mao, Chen, Comer, and Rutherford (2019) in *Costs and benefits of a shipping emission control area in the Greater Pearl River Delta region.*[1] Using a geospatial, hourly ship emissions inventory from 2015 (Olmer, Comer, Roy, Mao, & Rutherford, 2017), we projected these emissions to 2030 and estimated how a 200-nautical mile (nm) Emission Control Area (ECA) along the coast of China could reduce air pollution and improve air quality and public health. Emission reductions were translated to air quality improvements using the widely accepted regional chemical transport model Weather Research and Forecasting, which we combined with Chemistry (WRF-Chem). Health-related benefits were modeled with a log-linear concentration-response function that links changes in air pollution concentration with health endpoints. These benefits were then compared with compliance costs to shipowners.

2. Detailed methodology

2.1 Emissions inventory

Baseline emissions were estimated for 2015, at which time no regional policies to control oceangoing vessel (OGV) emissions were in effect in China. Olmer et al. (2017) provides a step-by-step, detailed methodology that explains how raw automatic identification system (AIS) and ship technical data are used to develop air pollution and greenhouse gas (GHG) inventories. We retrieved the 2015 inventory using the ICCT Systematic Assessment of Vessel Emissions (SAVE) model. The SAVE model is a Python-based tool used to generate activity-based emission inventories based on ship activity data produced by the AIS and vessel characteristics data.[2]

Based on the geospatial baseline emissions inventory in 2015, we projected future shipping emissions in 2030 under two scenarios: business as usual (BAU) and with a 200-nm Chinese ECA. This allowed us to connect emission reductions from the ECA policy with improvements in ambient air quality and public health. The ECA extending 200 nm from China's coastline (shown in Figure 1) that we evaluated also allows for a direct comparison of results with the North American ECA. The delineation of a practical or most cost-effective Chinese ECA is beyond the scope of this study, but an analysis of potential ship rerouting for ECAs narrower than 100 nm is covered in Mao and Rutherford (2018).

Figure 1 captures the study region for this analysis. Domain 1 (resolution: 36 × 36 km per grid cell) is also the largest and most coarse domain for the transport-and-fate model. Two nested domains (Domain 2 and Domain 3) have finer resolutions of 12 × 12 km and 4 × 4 km per grid cell, respectively.

[1] The report can be found on ICCT's website at www.theicct.org/publications/pearl-river-delta-eca-201907

[2] Our AIS data vendor is exactEarth Ltd. and our ship registry data vendor is IHS Fairplay.

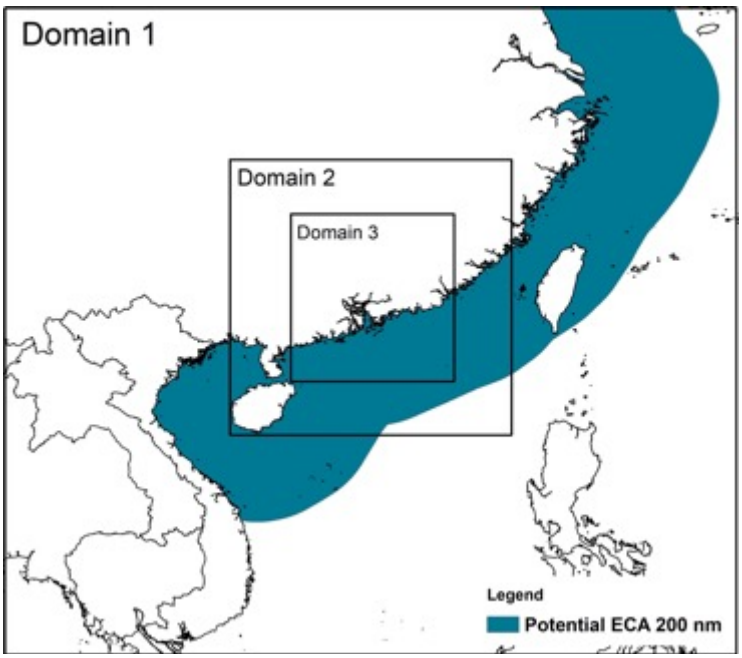

Figure 1. Study region, with three domains defined for air quality modeling.

In order to project a gridded 2030 emissions inventory, we developed several unitless scaling factors. These inflate the gridded hourly emissions of the baseline 2015 inventory to reflect three factors: future traffic growth, the fleet's fuel efficiency improvement, and environmental regulations. The overall equation for projection can be described as follows:

$$E_{i,j,2030} = \sum_{t=0}^{t=n}(E_{i,j,2015} * TSF_k * EAF_k * PAF_{j,l}) \quad (1)$$

Where:

i	= ship i
j	= pollutant j
k	= ship class k, to which ship i belongs
l	= ship engine type l, which corresponds to ship i
$E_{i,j,2030}$	= emissions (g) for ship i and pollutant j in 2030
$E_{i,j,2015}$	= emissions (g) for ship i and pollutant j in 2015
TSF_k	= trade scaling factor for ship class k
EAF_k	= efficiency adjustment factor for ship class k
$PAF_{j,l}$	= policy adjustment factor for pollutant j and engine type l

2.1.1 Trade scaling factor

Trade scaling factors (TSF_k) are defined as the impact of trade growth on ship emissions, holding everything else constant. As trade grows, demand for shipping activity grows, and so does energy use and air pollution. This increased demand can be met by introducing more ships or

making existing ships travel more frequently, or a combination of both. For simplicity's sake, in this modeling we assumed that the fleet adjusts by making more frequent trips. Based on Equation 2, which calculates the number of trips required to move a certain cargo type by the corresponding ship class, the growth rate in trade volume is essentially the growth rate in annual trips made to move that specific cargo, holding everything else constant.

$$N_k = \frac{V_k}{DWT_k * LF} \quad (2)$$

Where:

k	= ship class k, with corresponding cargo type k
N_k	= total number of trips made to move cargo type k
V_k	= total volume of cargo type k to be moved, tonnes
DWT_k	= deadweight tonnage of ship class k, maximum volume of cargo that can be carried, tonnes
LF	= load factor, unitless, ratio of the actual volume of cargo carried to *DWT*, assumed to be 0.75 across different ship classes

With the additional assumption that 2030 ship speeds are equal to those in 2015, the change in annual number of trips directly impacts the total annual fleet activity, measured in hours. Because the SAVE model calculates ships' fuel consumption using Equation 3, the trade growth impacts fuel consumption, and thus emissions, via the change in ship activity n.

$$FC_i = \sum_{t=0}^{t=n} (P_{demand,i} * 1\ hour) * EF_{energy,CO_2} / EF_{fuel,CO_2} \quad (3)$$

Where:

n	= annual activity (hours) for ship i
FC_i	= annual fuel consumption for ship i
$P_{demand,i}$	= hourly power demand (kilowatt, or kW) for ship i
EF_{energy,CO_2}	= energy-based CO_2 emissions factor, in grams per kW hour (g/kWh)
EF_{fuel,CO_2}	= fuel-based CO_2 emissions factor (g CO_2/g fuel)

Trade scaling factors (TSF_k) are cargo-specific trade growth rates from 2015 to 2030. Our trade forecast model estimated trade growth rates from 2015 to 2030 based on historical data published by the United Nations Conference on Trade and Development (UNCTAD, n.d.).

UNCTAD publishes seaborne trade volume by region and by major cargo type annually. For our study region, we looked at UNCTAD's data for Asian developing countries from 2006 to 2015 and projected out to 2030.[3] During this period, world seaborne trade will continue to grow as economies become more and more interrelated and as transportation costs fall. Asia is expected to grow to be the center of international trade (Shanghai International Shipping Institute, 2015).

Containerized cargo and bulk cargo also have solid growth momentum, but their expansion will likely occur at a slower rate than overall trade activity. Growth in liquefied natural gas (LNG) transport should also accelerate, whereas crude oil trade is expected to slow in the long term.

[3] We selected 2006 as the start year as the statistical caliber changes over the years, and because since 2006 the key statistics we needed for projection remained constant.

However, when we tried to fit historical data with a trend line and predict out to 2030, we found cases where the trend lines that were statistically the best fit did not reflect consensus projections for future activity. To rectify our extrapolation method with long-term projections, we used the following approach:

1. Fit the historical data with trendlines using both power and linear functions. The two resulting growth rates from 2015 to 2030 are set as the ICCT's lower (of the power and linear, whichever is smaller) and upper (of the power and linear, whichever is larger) bound of this analysis.
2. UNCTAD provides a long-term outlook for maritime transport in its 2017 report, and it includes cargo-specific trade growth estimates from multiple sources. We used those data to set low, medium, and upper bounds of third-party estimates.
3. Among these five growth rates, we then chose the one that is the average of the ICCT-extrapolated results, as summarized in Table 1. In two cases where our modeled rates were on the higher end— for liquefied bulk carriers and for crude oil tankers—the medium value from UNCTAD's reference was chosen.
4. The cargo growth rates were then assigned to ship classes, as summarized in Table 2.

Table 1. Trade growth rates for different cargo types from 2015 to 2030

Cargo type	Annualized growth rate						Total growth rate
	UNCTAD referenced (2017)			ICCT extrapolated		Chosen	2015–2030
	low	medium	high	low	high		
Containerized cargo	4.6%	4.8%	5.0%	2.8%	8.2%	5.5%	120%
Major dry bulk	3.6%	4.6%	5.6%	2.5%	3.4%	3.0%	56%
Liquified natural gas	1.7%	2.2%	2.7%	2.5%	4.0%	3.3%	62%
Crude oil	1.2%	1.9%	2.5%	0.0%	3.3%	1.9%	32%
Liquid bulk	1.7%	2.1%	2.5%	2.5%	2.5%	2.1%	37%
General cargo	2.7%			2.6%	5.0%	3.8%	75%
Cargo-other	2.7%			2.6%	5.0%	3.8%	37%
Passenger	2.7%			2.6%	5.0%	3.8%	75%

Table 2. Assignment of cargo types to major ship classes

Cargo type	Ship class
Containerized cargo	Container ships
Major dry bulk cargo, like coal, grain, and ores	Bulk carriers
Crude oil, and petroleum products	Oil tankers
Liquified natural gas	LNG carriers
Minor dry bulk cargo, like steel, minerals and agribulks	General cargo ships
Organic or inorganic chemicals	Chemical tankers

2.1.2 Efficiency adjustment factors (EAF_k)

Efficiency adjustment factors (EAF_k) capture reductions in air pollution due to fleetwide energy efficiency improvements. These include a baseline efficiency gain due to natural fleet turnover and additional benefits from the Energy Efficiency Design Index (EEDI) mandates set by the International Maritime Organization (IMO).

Even without regulations, newer ships would naturally be more energy efficient than older ones, because fuel savings are economically attractive to carriers. Our fleet-turnover model is adapted from the one used in the technical support document for the North American ECA application (U.S. Environmental Protection Agency [EPA], 2009), with the following assumptions:

- Technical data for the baseline fleet in 2015 is taken directly from the IHS Fairplay ship database
- The total number of ships remains unchanged over time[4]
- A ship's useful life is 25 years
- Each year, ships that reach the end of their useful life are replaced with new ships built in that year that have average ship characteristics of the existing fleet

The model output is a series of fleet profiles for each year from 2015 to 2030. For ships that appeared in our study region in 2015, relevant fleet characteristics for 2015 and 2030 are summarized in Table 3.

[4] In reality, increased transport demand through 2030 would be met by some combination of greater ship size, increased operational hours, and more ships. For simplicity's sake, we held the number of ships constant and assumed that additional supply was provided by increasing only ship size and hours at sea. This approach should somewhat underestimate the number of new ships brought into service in the future. As a consequence, there may be small second-order effects on the results that come from underestimating fuel efficiency gains through the EEDI and Tier III NO_x compliance rates from new-build ships after the ECA takes effect in 2025.

Table 3. Average ship characteristics by ship class in 2015 and 2030

Ship class	Capacity bin	Average ship characteristics							
		Main engine power (kW)		Deadweight tonnage (tonnes)		Length (m)		Design speed (knots)	
		2015	2030	2015	2030	2015	2030	2015	2030
Container ship	1	5,790	6,150	8,840	9,430	126	130	16	16.3
	2	12,000	12,000	19,200	18,500	166	162	18.9	18.9
	3	21,000	21,400	34,500	35,100	208	210	21.4	21.6
	4	35,500	34,700	54,400	53,900	263	259	23.4	23.3
	5	52,900	41,300	73,700	68,300	289	266	24.7	22.8
	6	60,200	60,100	109,000	109,000	330	329	24.3	24.3
	7	65,900	65,900	150,000	150,000	366	366	24	24
	8	61,700	61,700	182,000	182,000	395	395	20.4	20.4
Bulk carrier	1	1,720	1,710	4,790	4,990	92.3	93.5	11.5	11.4
	2	5,790	5,790	27,600	28,100	168	169	13.8	13.7
	3	8,330	8,420	50,800	51,400	189	189	14.3	14.3
	4	9,980	10,100	76,900	78,900	223	218	14.4	14.3
	5	17,000	17,200	171,000	172,000	287	287	14.5	14.5
	6	20,100	19,900	244,000	239,000	315	313	14.6	14.6
General cargo ship	1	1,280	1,230	2,820	2,870	80.6	80.9	11.2	11.1
	2	3,120	2840	7,180	7,030	108	109	12.7	12.4
	3	7,200	5,580	24,900	18,700	159	139	14.4	13.6
Chemical tanker	1	1,850	1,900	3,220	3,400	86.3	88.6	12.2	12.1
	2	3,210	3,010	7,620	7,450	112	112	13	12.8
	3	4,890	4,880	15,300	15,400	135	136	13.8	13.8
	4	8,710	7,320	43,500	35,200	180	164	14.7	14.3
Oil tanker	1	1,640	1,590	3,130	3,180	83.3	83.3	11.6	11.4
	2	2,800	2,790	6,830	6,810	108	109	12.5	12.4
	3	4,010	4,150	14,300	14.700	139	143	12.8	12.9
	4	8,900	9,070	45,300	45,900	183	182	14.6	14.7
	5	12,100	12,100	74,000	74,400	228	228	14.9	14.9
	6	13,500	13,700	109,000	110,000	245	246	14.9	14.9
	7	17,700	15,400	156,000	140,000	274	240	15.3	14.7
	8	27,500	28,000	308,000	310,000	333	333	15.6	15.6
Liquified gas tanker	1	3,920	4,220	7,030	7,830	110	114	14.2	14.4
	2	22,800	20,300	68,900	60,000	260	235	18.2	17.5
	3	36,900	36,900	122,000	122,000	326	326	19.2	19.2
Cruise ship	2	7,030	7,730	1,250	1,370	111	115	16	16.1
	3	19,100	29,900	3,650	5,190	186	206	19.3	19.8
	4	54,700	63,700	8,260	9,310	270	290	22.6	21.9
	5	75,100	67,200	12,300	9,770	309	308	22.6	21.4
Roll-on/roll-off	1	2,780	1,700	2,800	2,010	81.8	69.2	11.5	10.3
	2	12,400	11,800	17,400	19,900	172	171	18	16.6
Refrigerated bulk carrier	—	4,680	4,170	5,990	5,480	115	111	15.8	15.4
Vehicle carrier	—	13,400	13,600	18,300	18,400	193	194	19.6	19.6
Tug boat	—	3,390	3,520	357	372	37.9	38.1	12.5	12.6
Fishing boat	—	1,680	1,700	590	603	61.9	62.3	12.2	12.1

As shown in Table 3, as ships retire and are replaced by new ships, the fleet becomes naturally more efficient. This is because newer ships tend to be bigger and have newer engines that burn less fuel while doing the same amount of transport work. According to Equation 2 and Equation 3, the increase in the fleet's deadweight tonnage (DWT_k, a surrogate for fleet cargo-carrying capacity) and the increase in the fleet's engine power ($P_{demand,i}$) affect total fuel consumption in opposite ways. That is, higher DWT_k tends to reduce the total number of trips needed to move the cargo and $P_{demand,i}$ increases the amount of fuel consumed per trip.

Additionally, 2030 fleetwide efficiency very likely will outperform natural improvement due to incentives provided by IMO regulations like the EEDI. The EEDI mandates that ships built after a certain date be more energy efficient than the baseline fleet in terms of g CO_2/tonne-mile (International Maritime Organization, 2016). For example, ships built after 2025 need to be 30% less carbon intensive than a predefined EEDI baseline (Hon & Wang, 2011)[5]. Assuming a gradually decreasing survival rate for a fleet with increasingly longer in-service history (Wang & Lutsey, 2013), we estimated that implementing current EEDI standards alone would reduce the fuel intensity of an average ship by about 20% in 2030 compared to 2015 levels. As a result, we adopted this number to construct the efficiency adjustment factor. This assumption is similar to the 22.5% figure used for the *Third IMO Greenhouse Gas Study* (Smith et al., 2015) to account for the EEDI's impact on projected emissions in 2030.

As a result, the efficiency adjustment factors (EAF_k) are calculated with the following equation:

$$EAF_k = \frac{P_{k,2030}}{P_{k,2015}} * \frac{DWT_{k,2015}}{DWT_{k,2030}} * (1 - 20\%) \quad (4)$$

Where:

$P_{k,2030}$ = average power demand (kW) for ship class k in 2030

$P_{k,2015}$ = average power demand (kW) for ship class k in 2015

$DWT_{k,2015}$ = average deadweight tonnage, surrogate for cargo carriage per voyage, for ship class k in 2015

$DWT_{k,2030}$ = average deadweight tonnage, surrogate for cargo carriage per voyage, for ship class k in 2030

2.1.3 Policy adjustment factors ($PAF_{j,l}$)

Emission factors, which are linked with fuel consumption, determine the amount of emissions for different pollutants. They vary by ship engine type and fuel type, and are influenced by environmental regulations. ECAs are designed to control conventional air pollutants including sulfur oxides (SO_x), nitrogen oxides (NO_x), and particulate matter (PM). Therefore, projections of future emissions of these pollutants need to be adjusted for future changes in environmental policies.

Policy adjustment factors are defined as ratios of emission factors under 2030 scenarios (BAU scenario and ECA-control scenario) compared to the 2015 baseline for each pollutant. Unlike trade scaling factors and efficiency adjustment factors, policy adjustment factors vary by location for different scenarios. Within SAVE, a location identifier representing one of the following locations relevant to a Chinese ECA is assigned to each grid cell:

- ❑ At berth
- ❑ Within 12 nm around Hainan Island

[5] The EEDI standards are recently tightened. IMO moved up the start date of Phase 3 of its Energy Efficiency Design Index (EEDI) standards for new ships by three years, from 2025 to 2022, for five ship types. Details can be found here: https://theicct.org/blog/staff/mepc74.

- ❑ Within the 200-nm ECA
- ❑ Outside of the 200-nm ECA

Table 4 summarizes all $PAF_{j,l}$s for this analysis, and the following sections explain in detail how those adjustment factors were derived for each pollutant.

Table 4. Policy adjustment factors for SO_x, PM_{10}, and NO_x in emissions projection

Pollutants	Scenarios	Locations	**Policy adjustment factors**		Underlying policies
			2015	**2030**	
SO_x	ECA-control	Inside ECA	1	**0.04**	Fuel sulfur content ≤ 0.1% m/m
		Outside ECA		**0.2**	Fuel sulfur content ≤ 0.5% m/m
	BAU	At berth	1	**0.04**	Fuel sulfur content ≤ 0.1% m/m
		All other		**0.2**	Fuel sulfur content ≤ 0.5% m/m
PM_{10}	ECA-control	Inside ECA	1	**0.11–0.17**	Fuel sulfur content ≤ 0.1% m/m
		Outside ECA		**0.48–0.55**	Fuel sulfur content ≤ 0.5% m/m
	BAU	At berth	1	**0.11–0.17**	Fuel sulfur content ≤ 0.1% m/m
		All other		**0.48–0.55**	Fuel sulfur content ≤ 0.5% m/m
NO_x	ECA-control	Inside ECA	1	**0.2–0.25**	Ships built after 2025 complying with Tier III
		Outside ECA		**0.79–1**	All ships complying with Tier II or Tier I
	BAU	At berth	1	**0.79–1**	All ships complying with Tier II or Tier I
		All other			All ships complying with Tier II or Tier I

2.1.3.1 Sulfur oxides

Emission factors for SO_x are determined by fuel sulfur content as shown in Equation 5. Currently, the global average sulfur content for marine fuel is around 25,000 ppm (Smith et al., 2015). Proposed environmental policies that will impact future fuel sulfur content include the following:

- ❑ The IMO 2020 global sulfur limit. Starting in 2020, all IMO-regulated vessels must use fuel with less than 5,000 ppm sulfur content globally.[6] This will result in an 80% reduction in the SO_x emission factor from 2015 to 2030 in the BAU scenario.
- ❑ China's national domestic emission control area (DECA) policy. Starting in 2019, all ships operating within China's territorial waters (i.e., within 12 nm of its coastal baseline) must use fuel that comports with the IMO's post-2020 sulfur limit. In addition, all ships traveling within two inland waterway systems and within 12 nm of Hainan Island will need to use marine fuel with less than 1,000 ppm sulfur content starting in 2020 and 2022, respectively.[7] When our analysis took place, China's national DECA policy was not final yet. The proposal at that time included a requirement that ships burn 1,000 ppm sulfur fuel while berthing at ports within the DECA region, and it was taken out of the final rule. Our analysis, which was based on the proposal, is thus overestimating the

[6]Almost all OGVs apply this rule. The few exceptions include, but are not limited to, fishing vessels, leisure ships, research, and rescue ships.

[7] The two inland waterway systems are the Yangtze River and the Pearl River.

effectiveness of the national DECA policy in reducing SO_x and PM_{10} emissions, but only slightly.

Equation 5 summarizes the relationship between the sulfur content of marine fuel and its resulting SO_x emission factor.

$$EF_{fuel,SO_x} = 2 * 0.97753 * SC_{fuel} \quad (5)$$

Where:

$fuel$	= fuel type
2*0.97753	= 0.97753 is the fraction of fuel *S* converted to SO_x and 2 is the ratio of molecular weight of SO_x and *S*
EF_{fuel,SO_x}	= fuel-based emissions factors for SO_x, in *g* (SO_x)/*g* (fuel)
SC_{fuel}	= sulfur content (% m/m) of a certain fuel

If a 200-nm Chinese ECA is in place in 2030, then the entire region will enforce the 1,000 ppm fuel sulfur requirement. Thus, the 96% reduction in the SO_x emission factor was applied to the whole ECA region for the ECA-control scenario.

2.1.3.2 Particulate matter (PM_{10})

Similar to SO_x, the PM_{10} emission factor is related to fuel sulfur content as shown in Equations 6 and 7.[8] As a result, policies that reduce SO_x naturally have a spillover effect on PM_{10}, even if PM_{10} is not a direct target. Since PM_{10} emission factors are also related to ship specific fuel oil consumption (SFOC)s, the impacts of policy on PM_{10} emission factors are also ship-specific. On average, the IMO 2020 global sulfur limit will result in a 50% reduction in the PM_{10} emission factor and the ECA's sulfur limit will reduce the PM_{10} emission factor by approximately 90%.

$$EF_{energy,PM_{10},HFO} = 1.35 + SFOC * 7 * 0.02247 * (SC_{HFO} - 0.0246) \quad (6)$$

Where:

HFO	= heavy fuel oil, or residual oil
$EF_{power,PM_{10},HFO}$	= energy-based PM emissions factor (g/kWh) of heavy fuel oil (HFO)
$SFOC$	= specific fuel oil consumption, *g* (fuel)/kWh, a value specific to engine types
SC_{HFO}	= sulfur content (% m/m) of HFO

$$EF_{energy,PM_{10},MGO} = 0.23 + SFOC * 7 * 0.02247 * (SC_{MGO} - 0.0024) \quad (7)$$

Where:

MGO	= marine gas oil, or distillate fuel
$EF_{power,PM_{10},MGO}$	= energy-based PM emissions factor (g/kWh) of marine gas oil (MGO)
SC_{MGO}	= sulfur content (% m/m) of MGO

The $SFOC$s used to convert energy-based emission factors to fuel-based emission factors in this analysis are included in Table 5, which is adapted from Smith et al. (2015).

[8] PM_{10} is considered to be equivalent to PM in terms of emission factors (Smith et al., 2015). We did not evaluate direct tailpipe $PM_{2.5}$ emissions, but their emission factors can be understood as 92% of PM_{10} (U.S. EPA, 2009).

Table 5. SFOC assumptions

Engine type	Engine	Fuel type	SFOC (g/kWh)
Main diesel engine	Slow-speed diesel	HFO	195
		MGO	185
	Medium-speed diesel	HFO	215
		MGO	205
	High-speed diesel	HFO	215
		MGO	205
Gas turbine	n/a	HFO	305
		MGO	300
Steam turbine	n/a	HFO	305
		MGO	300
LNG engine	n/a	LNG	166
Auxiliary diesel engine	Medium- and high-speed diesel	HFO	227
		MGO	217

2.1.3.3 Nitrogen oxides

Determining NO_x emission factors is a bit more complicated because the IMO regulates NO_x by "Tier" according to when the ship was built. Therefore, the projection used here combines the fleet turnover model, which outputs the fleet's age distribution in any future year, with scaling factors for NO_x emission factors by ship class and geography (i.e., within or outside of an ECA).

All ships built after 2011 should be IMO Tier II compliant. The IMO Tier III regulations apply only in ECA regions, and to ships built after the effective date of each individual ECA, if that date is not earlier than 2016. For example, the North American ECA, effective since 2012, requires that ships built after 2016 be Tier III compliant when sailing in its region. The North Sea and Baltic Sea ECAs, meanwhile, require that ships built after 2021 be Tier III compliant when sailing within their regions.

Tier III compliance is achieved primarily by installing NO_x aftertreatment devices—either selective catalytic reduction (SCR) or exhaust gas recirculation (EGR)—on Tier II engines. Both technologies have been successfully demonstrated on OGVs, but with varying cost implications. SCR is less well suited than EGR for low-load operation and maneuvering in coastal and harbor areas; this is due to poor efficiencies at low exhaust temperatures. In the 2030 BAU scenario, no ships in our study region would be Tier III compliant. Ships that are Tier III compliant in other ECAs around the world can opt to shut down their NO_x aftertreatment devices while navigating outside of designated ECAs. This returns them to Tier II status while keeping them "Tier III ready." For the Chinese ECA scenario, we assumed that the 200-nm ECA entered into effect starting in 2025, meaning that only new ships built after 2025 that visited our study region need to be "Tier III ready" and Tier III compliant when entering the ECA.

IMO NO_x tier limits are set as a function of engine speed in revolutions per minute (rpm). With the fleet turnover model, each new-build ship was assigned an engine rpm averaged across the same engine type and ship class of the introduction year. With the build year and engine rpm, its NO_x emission factor can be determined accordingly. Thus, the fleetwide impact of NO_x emission factors can be summarized by ship class and then applied to the gridded baseline emissions inventory (see Table 6).

Table 6. Average NOx emission scaling factors by ship class, 2030

Ship class	Average $PAF_{j,l}$ for NO_x emission factor
Container ship	0.94
Bulk carrier	0.96
General cargo ship	0.92
Chemical tanker	0.95
Oil tanker	0.90
Liquified gas tanker	0.95
Cruise ship	0.80
Roll-on/roll-off	0.92
Refrigerated bulk carrier	0.84
Vehicle carrier	0.95
Tug boat	0.91
Fishing vessel	0.80

2.1.3.4 Other pollutants

Although ECA policy targets only SO_x, NO_x, and PM_{10} emissions, we calculated emissions for other major pollutants as inputs into air quality modeling.

- ❏ Carbon dioxide (CO_2): The ECA policy does not impact CO_2 emission factors.
- ❏ Carbon monoxide (CO): The ECA policy does not impact CO emission factors.
- ❏ Black carbon (BC): BC emission factors change with fuel type. ECA fuel sulfur regulations will be mostly achieved by switching to cleaner fuel types, and this will have an impact on BC emission factors. BC emission factors associated with different fuel types can be found in Comer, Olmer, Mao, Roy, and Rutherford (2017).
- ❏ Methane (CH_4): The ECA policy does not impact CH_4 emission factors.
- ❏ Nitrous oxide (N_2O): N_2O emission factors slightly change with fuel type. When switching from HFO to MGO, N_2O emission factors increase to 0.0016 (g pollutant/g fuel) by about 6.25%.
- ❏ Non-methane volatile organic compound (NMVOC): The ECA policy does not impact NMVOC emission factors.

2.2 Air quality modeling

To evaluate the impacts of a Chinese ECA on ambient air quality, we used air quality modeling to simulate concentrations of key air pollutants in 2030. Before describing the model, below, we first explain the relevant policy scenarios and key underlying assumptions. We used the regional chemical transport model WRF-Chem (Grell et al., 2005) version 3.5 for the ambient air quality estimation. The details of the model setup and key parameters are consistent with Chen et al. (2019). The model was run three times with different inputs, as described in Table 7.

Table 7. Scenarios and assumptions for air quality modeling

Scenario	Name	Inputs	Emission control policies for ships

S1	2030 without ship emissions	2030 land emissions	N/A
S2	2030 BAU	2030 land emissions, 2030 baseline ship emissions	SO_x and PM: IMO 2020 global sulfur limit and China national DECA NO_x: IMO Tier II
S3	2030 ECA-control	2030 land emissions, 2030 control ship emissions	SO_x and PM: IMO 2020 global sulfur limit and China 200-nm ECA NO_x: IMO Tier III for ships built after 2025

The WRF-Chem model simulated air quality within the three domain sizes, all centered at the Greater Pearl River Delta (GPRD) region (see Figure 1). The largest model domain, with a 36 × 36 km horizontal grid, covers half of Eastern China and neighboring South Asian countries. Two nested domains have finer resolutions of 12 × 12 km and 4 × 4 km, respectively. All three domains have 31 vertical levels, from the surface to 50 millibar atmospheric pressure. We used specified initial and lateral boundary conditions from the MOZART-4 global chemical transport model (Emmons et al., 2010), to account for the initial and background chemical concentrations.

2.2.1 Meteorological data

Due to the lack of future meteorological data, the model input the 6-h temporal resolution meteorological data from the Global Forecast System for the year of 2015 (National Centers for Environmental Prediction, n.d.). The simulated horizontal winds, temperature, and humidity were nudged to the respective meteorological fields. To find the upper bound impacts on air quality from ship emissions, we modeled the month of July, which is the monsoon season and when southeastern winds transport ship emissions from the sea to the land (Lu et al., 2009). It is likely that the impacts from ship emissions on the GPRD cities are at their maximum during this season. Some studies also have shown that the highest contributions of ship emissions toward land occur in July (Chen et al., 2018; Liu et al., 2018). The time period of the model simulation was the entire month of July, with four spin-up days from June 27 to June 30. The model generated hourly concentrations for every simulation day. Further analysis, including model evaluation and monthly average concentrations of pollutants, was based on the daily average concentrations from July 1 to July 31.

2.2.2 Chemical mechanisms

The model used the Regional Acid Deposition Model version 2 (RADM2) from Stockwell, Middleton, Chang, and Tang (1990) for the gas-phase chemical mechanism to predict the highly nonlinear ozone, sulfate, nitric acid, and hydrogen peroxide concentrations under various atmospheric conditions. For aerosols in the atmosphere, we used the Modal Aerosol Dynamics Model for Europe with the Secondary Organic Aerosol Model (MADE/SORGAM) (Ackermann et al., 1998; Schell et al., 2001). MADE/SORGAM accounts for the aerosol dynamics, including formation (i.e., condensation, nucleation, coagulation), transport, dry deposition, and aerosol-cloud interaction. MADE/SORGAM further predicts the mass of several particulate-phase species, including sulfate, ammonium, nitrate, sea salt, dust, black carbon, organic carbon and secondary organic aerosols in the three log-normal aerosol modes: Aitken, accumulation, and coarse. Photochemistry in the atmosphere was simulated by photolysis of key species. Photolysis rates were obtained from the Fast-J photolysis scheme (Wild, Zhu, & Prather, 2000) which was

strongly affected by clouds and aerosols. All meteorological fields and chemical mechanisms stayed the same for both years (2015 and 2030).

2.2.3 Emission inputs

The ship emissions inventory was described in the previous section. For land-based emissions within China in 2015, we used the Multi-resolution Emission Inventory of China (MEIC).[9] For 2015 emissions in the part of Domain 1 that are outside of China, we used the Regional Emission Inventory in ASia version 2 (REAS) (Kurokawa et al., 2013). Both MEIC and REAS inventories provide emissions of major primary and secondary air pollutant precursors, including NO_x, SO_2, volatile organic chemicals (VOCs), ammonia (NH_3), CO, and PM. PM in both inventories is classified by OC, BC, $PM_{2.5}$ and PM_{10}. For 2030, we chose the 2030-With Additional Measures anthropogenic emissions projection produced by Cai et al. (2018), which is based on a 2013 emission inventory by Ma et al. (2017). For 2030 emissions in Domain 1 outside of China, we used the Representative Concentration Pathway 8.5 emission inventory for the rest of the East Asia region from Riahi et al. (2011). The WRF-Chem model used the Model of Emissions of Gases and Aerosols from Nature version 2.1 (Guenther et al., 2012) for biogenic emissions based on the weather and land-use data. WRF-Chem calculated the dust and sea salt emissions online by using the dust transport model (Shaw et al., 2008) and sea salt schemes (Gong, 2003). Aircraft emissions of BC, CO, OC, $PM_{2.5}$, NO_x, and SO_2 were added from the Task Force Hemispheric Transport of Air Pollution emissions inventory (Janssens-Maenhout et al., 2015).

2.2.4 Air quality model performance evaluation

The model was evaluated by comparing modeled pollution concentrations in 2015 with observed concentrations from monitoring stations. Performance was determined by statistical metrics including the correlation coefficient (r), the normalized mean bias (NMB), the normalized mean error (NME), the mean fractional bias (MFB), the mean fractional error (MFE), and the root mean square error (RMSE) between the observed measures and modeled outputs (Chang & Hanna, 2004). Table 8 summarizes the model performance related to meteorological parameters (Chen et al., 2019).

Table 8. Summary statistics for the four meteorological variables modeled and observed in four cities of the PRD region

Variable	Site	Normalized mean bias (%)	Normalized mean error (%)	Mean fractional bias (%)	Mean fractional error (%)	Correlation coefficient	Root mean square error
2-meter Temperature	Guangzhou	0.3	0.3	0.1	0.1	0.9	1.2
	Shenzhen	0.2	0.3	0.1	0.1	0.8	1.1
	Zhaoqing	-0.3	0.4	-0.1	0.1	0.7	1.6
	Hong Kong	0.0	0.2	0.0	0.1	0.8	0.9
10-meter Wind Speed	Guangzhou	-15.0	17.6	-4.4	5.1	0.9	0.6
	Shenzhen	-36.4	36.4	-11.2	11.2	0.8	2.0

[9] More detailed information on MEIC can be found at http://www.meicmodel.org

	Zhaoqing	31.6	39.9	5.9	8.0	0.5	1.0
	Hong Kong	-35.9	35.9	-11.0	11.0	0.8	1.9
10-meter Wind Direction	Guangzhou	-9.8	21.0	-2.7	5.6	0.5	45.7
	Shenzhen	-0.8	11.9	-0.7	3.2	0.8	30.7
	Zhaoqing	-5.9	21.1	-0.8	5.6	0.5	47.3
	Hong Kong	11.2	17.8	2.2	4.1	0.6	46.4
Surface Relative Humidity	Guangzhou	-15.9	16.4	-4.7	4.9	0.5	17.0
	Shenzhen	-12.3	15.1	-3.8	4.5	0.6	15.9
	Zhaoqing	-1.6	9.1	-0.6	2.4	0.5	10.1
	Hong Kong	-2.6	11.2	-1.1	3.1	0.7	11.2

The model slightly underestimated the relative humidity in all four selected sites, as well as the wind speed in Guangzhou, Shenzhen, and Hong Kong. The model, however, overestimated the wind speed at Zhaoqing, with a correlation of 0.5 and NMB of 32%. Figure 2 shows the comparison between observed and modeled wind. The length of each wedge shows the number of hours that were observed or modeled within that direction (i.e., the direction from which the wind comes). The pattern shows that southerly wind was the most dominant, indicating that wind most often blew from the ocean to the land.

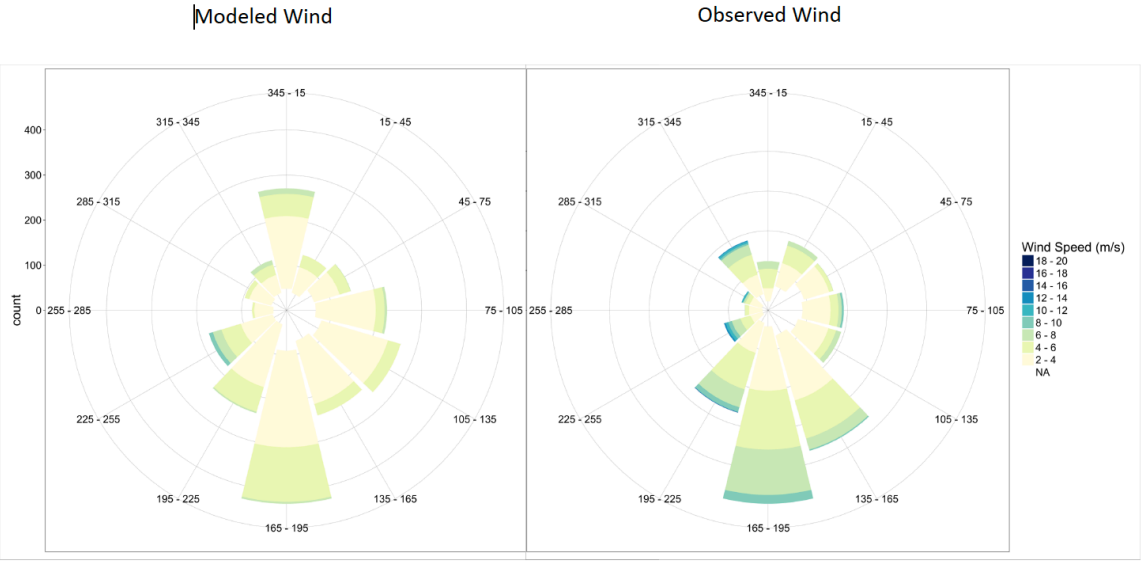

Figure 2. Modeled versus observed wind speed and wind direction.

We evaluated the model performance of $PM_{2.5}$ based on the standards developed by Boylan and Russell (2006), which set the performance goals for $PM_{2.5}$ at MFB less than or equal to ±30% and MFE less than or equal to 50%. The performance criteria for $PM_{2.5}$ were set at MFB less than or equal to ±60% and MFE less than or equal to 75%. For ozone (O_3), both MFB and MFE were set at less than or equal to ±15% and 35%, as recommended by Morris et al. (2007).

Figure 3 and Table 9 summarize the modeled versus observed daily mean $PM_{2.5}$ and O_3 concentrations. As shown in the graphs, the model somewhat overestimated $PM_{2.5}$ concentrations in some cities, including Guangzhou and Shenzhen. This might be due to underestimated wind

speed and precipitation. As previously mentioned, we found that the modeled wind speed is less than the observed wind speed, which could predict more stagnant air in some cities (see Figure 2). Nevertheless, the $PM_{2.5}$ model performance for all cities still met the goal of MFB ≤ ±30% and MFE ≤ ±50%; the model performance of O_3 concentrations also met the goals of MFB ≤ ±15% and MFE ≤ ±35%.

Figure 3. Modeled versus observed daily mean $PM_{2.5}$ and O_3 concentrations in nine GPRD cities.

Table 9. Summary statistics for two pollutant concentrations for the model evaluation

	City	Normalized mean bias (%)	Normalized mean error (%)	Mean fractional bias (%)	Mean fractional error (%)	Correlation coefficient	Root mean square error
$PM_{2.5}$	Guangzhou	193.3	197.4	20.3	21.5	0.5	81.6
	Shenzhen	245.3	245.3	24.3	24.3	0.3	62.6
	Zhuhai	86.6	98.4	10.1	14.5	0.6	26.8
	Foshan	53.6	71.8	7.9	12.4	0.5	36.2
	Zhongshan	195.2	195.3	20.8	20.8	0.4	58.2

	Jiangmen	209.1	211.8	18.7	19.5	0.4	54.1
	Dongguan	188.2	188.2	22.3	22.3	0.5	59.7
	Huizhou	199.5	199.9	24.5	24.6	0.5	49.1
	Zhaoqing	27.2	41.9	4.5	8.5	0.3	18.3
O_3	Guangzhou	-29.7	40.1	-6.2	10.5	0.5	69.1
	Shenzhen	-5.1	26.6	-0.3	6.1	0.5	37.2
	Zhuhai	-18.6	26.5	-2.9	5.7	0.8	43.4
	Foshan	-27.8	33.1	-7.0	8.6	0.7	53.1
	Zhongshan	-3.8	31.1	1.8	7.7	0.8	34.3
	Jiangmen	1.5	23.9	2.4	6.4	0.8	26.1
	Dongguan	-39.1	40.5	-10.8	11.5	0.7	73.3
	Huizhou	-3.2	19.8	0.0	5.1	0.8	23.2
	Zhaoqing	-26.8	30.5	-7.0	8.1	0.7	43.5

2.3 Health impact analysis

2.3.1 Mortality

We estimated the health impacts due to ship-caused $PM_{2.5}$ and O_3 increases for both acute (short-term) and chronic (long-term) mortality. For acute mortality, we calculated the total number of deaths from cardiovascular disease (CVD), and respiratory (RESP) mortality for both $PM_{2.5}$ and O_3. For chronic mortality, we calculated premature mortalities from ischemic heart disease (IHD), chronic obstructive pulmonary disease (COPD), lung cancer (LC), cerebrovascular disease (CEV), and RESP. The details of the health impact analysis are consistent with Chen., Saikawa., Comber., Mao., and Rutherford. (2019, in press).

Premature mortalities related to ship emissions were estimated by Equation 8 that links changes in air pollution concentrations to health endpoints:

$$\Delta y = y_0 * Pop * \left(1 - \frac{1}{e^{\beta*(C_1 - C_0)}}\right) \quad (8)$$

Where:

β = model parameterized slope of the log-linear relationship between concentration and mortality
Δy = change in premature mortality incidences
y_0 = baseline incidence rate of a given health endpoint
Pop = population
$C_1 - C_0$ = change in air pollution concentration, in $\mu g/m^3$

We found the upper and lower limits of mortality (95% of confidence interval) based on the upper and lower limits of β, which depends on the relative risk (RRs) of each health endpoint.

$$\beta = \frac{\ln(RR)}{\Delta c} \quad (9)$$

Where:

RR = relative risk, defined as the ratio of death incidence caused by the change of pollution exposure to death incidence among the nonexposed population

Δc = unit increase in air pollutant concentrations (10 μg/m^{3}or 10 ppb)

The RR is the ratio of the incidence of death among those exposed to the extra pollution ($PM_{2.5}$ or O_3 in this study) to that of the nonexposed population. We retrieved the acute RRs from two PRD-specific time series studies, Lin et al. (2016) and Tao et al. (2012), to estimate mortality for both $PM_{2.5}$ and O_3 exposure. These RRs only apply to six cities in the Pearl River Delta (PRD). They are Guangzhou, Shenzhen, Dongguan, Foshan, Jiangmen, and Zhuhai and thus, for the health impacts related to acute exposures for this study, we provided mortality estimates for only those six cities. Still, these cities account for nearly half of the population in the GPRD region, and that means our estimates should capture the largest health impacts.

We obtained the baseline incidence of short-term all-cause, CVD, and respiratory diseases for the six main cities in the PRD from the Guangdong Provincial Center for Disease Control and Prevention (Lin et al., 2016). Due to a lack of city-specific baseline incidence rates for chronic diseases, we applied the provincial baseline incidence rates in 2015 (personal communication with Health Effects Institute, October 2018) to all cities in Guangdong Province, and applied the standalone rates for Hong Kong only because of its special cultural and governmental settings from mainland China. For 2030 scenarios, only chronic mortality was predicted due to the lack of baseline incidence data. These values are summarized in Table 10.

Table 10. *B*aseline incidence rates per 1,000 people in the Pearl River Delta region.

	2015 Base Incidence Rate for Guangdong (per 1,000 people)	2030 Base Incidence Rate for Guangdong (per 1,000 people)	2015 Base Incidence Rate for Hong Kong (per 1,000 people)	2030 Base Incidence Rate for Hong Kong (per 1,000 people)
All Cause	6.5	8.5	8.9	11.6
CVD	2.8	3.7	2.8	3.7
CEV	1	1.3	0.6	0.8
IHD	1.3	1.7	0.6	0.8
COPD	0.6	0.8	1.2	1.6
RESP	0.1	0.1	0.8	1
LC	0.4	0.5	0.8	1
Hospital Admission	154	201	154	201
Outpatient Visits	5,616	7,329	5,616	7,329

For chronic mortality due to $PM_{2.5}$ exposures, the RRs can vary with different $PM_{2.5}$ concentrations. Thus, we adopted the long-term Integrated Exposure Response (IER) function to find the RRs under different $PM_{2.5}$ concentrations. This is the most recognized method to estimate chronic $PM_{2.5}$-related mortality. The IER function for each health endpoint was developed by Burnett et al. (2014). These values are widely used to estimate the global burden of disease attributable to $PM_{2.5}$ exposure around the world. The IER model is written as:

$$RR(z) = \begin{cases} 1, & z < z_{cf} \\ 1 + \alpha\left\{1 - e^{[-\gamma*(z-z_{cf})^{\delta}]}\right\}, & z \geq z_{cf} \end{cases} \quad (10)$$

Where:

α, γ, δ	= model parameters for each health endpoint, determined by fitting a curve to RR data taken from studies on ambient air pollution, secondhand tobacco smoke, household solid cooking fuel, and active smoking
$RR(z)$	= relative risk at the z exposure level
z	= $PM_{2.5}$ concentration, in $\mu g/m^3$
z_{cf}	= counterfactual concentration below which no additional risk is assumed

Because there are few cohort studies that were performed in China, and none of them was further validated, the IER functions are currently regarded as the best estimate of the long-term mortality. The IER functions are developed for causes of mortality including IHD, CEV, COPD, and LC.

Due to the lack of studies for the chronic mortality due to O_3 exposure, we simply adopted RRs from a cohort study by Jerrett et al. (2009) for CVD, RESP, and IHD. Unlike RRs developed by the IER model, a single set of RRs was used for O_3. This was consistent for all O_3 concentrations and age groups and, therefore, higher uncertainty might remain in the O_3 chronic mortality estimation than in the $PM_{2.5}$ chronic mortality estimation.

$$RR = e^{\beta * (z - z_{cf})} \tag{11}$$

Where:

β	= model parameterized slope of the log-linear relationship between concentration and mortality
RR	= relative risk of ground-level ozone exposure
z	= average 8-hour daily maximum ground-level ozone concentration, in $\mu g/m^3$
z_{cf}	= counterfactual concentration below which no additional risk is assumed

Table 11 summarizes the above RRs associated with a 10 $\mu g/m^3$ change in particulate matter or 10 ppb change in O_3 that are used for this analysis.

Table 11. Relative risks of premature mortality

Outcome and exposure metric	Relative Risks (95% CI)	Reference
All cause (natural) mortality and short-term exposure to $PM_{2.5}$	1.0176 (1.0147, 1.0206)	Lin et al., 2016
Cardiovascular mortality and short-term exposure to $PM_{2.5}$	1.0219 (1.0180, 1.0259)	Lin et al., 2016
Respiratory mortality and short-term exposure to $PM_{2.5}$	1.0168 (1.010, 1.0237)	Lin et al., 2016
All cause (natural) mortality and short-term exposure to O_3	1.0081 (1.0063, 1.010)	Tao et al., 2012
Cardiovascular mortality and short-term exposure to O_3	1.0101 (1.0071, 1.0132)	Tao et al., 2012
Respiratory mortality and short-term exposure to O_3	1.0133 (1.0089, 1.0176)	Tao et al., 2012
Ischemic heart disease and long-term exposure to $PM_{2.5}$	IER	Burnett et al. (2014)
Chronic obstructive pulmonary disease and long-term exposure to $PM_{2.5}$		
Cerebrovascular disease and long-term exposure to $PM_{2.5}$		
Lung cancer and long-term exposure to $PM_{2.5}$		
Ischemic heart disease and long-term exposure to O_3	1.015 (1.003, 1.026)	Jerrett et al., 2009
Respiratory mortality and long-term exposure to O_3	1.029 (1.010, 1.048)	Jerrett et al., 2009
Cardiovascular mortality and long-term exposure to O_3	1.011 (1.003, 1.023)	Jerrett et al., 2009

The baseline incidence rate (y_0) for each health endpoint in Guangdong Province and Hong Kong was retrieved from the provincial baseline incidence rate in 2015 (personal communication with Health Effects Institute, October 2018). Separately, we projected the 2030 base incidence rate by considering increases in crude death rates from 2015 to 2030 in China according to the UN Department of Economic and Social Affairs (n.d.). The gridded population data from 2015 were retrieved from the National Aeronautics and Space Administration's Socioeconomic Data and Applications Center's fourth version of its Gridded Population of the World (Center for International Earth Science Information Network, 2016) and were projected to 2030 gridded population based on a methodology developed by the UN Department of Economic and Social Affairs (United Nations, Department of Economic and Social Affairs, Population Division, 2017). The city-level population for both years and the total death incidences are in Table 12.

Table 12. 2015 and 2030 projected population and all-cause baseline mortality for cities in the GPRD region

City	2015 Population	2030 Projected Population	2015 Mortality (All cause)	2030 Projected Mortality (All cause)
Guangzhou	19,718,753	20,341,965	131,819	172,018
Shenzhen	15,456,921	15,945,437	103,329	134,840
Dongguan	12,235,261	12,621,956	81,792	106,735
Foshan	11,084,311	11,434,631	74,098	96,695
Hong Kong	9,506,476	9,806,929	87,291	113,911
Huizhou	7,520,142	7,757,816	50,272	65,603
Jiangmen	6,487,500	6,692,537	43,369	56,594
Zhaoqing	5,657,705	5,836,517	37,822	49,355
Zhongshan	4,604,145	4,749,659	30,779	40,165
Zhuhai	2,699,468	2,784,785	18,046	23,549
Macao	600,942	619,935	—[a]	—[a]
GPRD	95,571,624	97,972,232	658,617	859,465

[a] No estimate because too small to model with precision at Domain 3 scale.

2.3.2 Morbidity

We used the same function, Equation 8, to estimate the ECA-reduced morbidity for hospital admissions and outpatient visits. We first found the PM_{10} concentration difference between 2030 BAU and 2030 ECA-control scenario, then estimated the ECA's health benefits from reduced morbidity.[10]

Total hospital admissions and outpatient visits for China were retrieved from Fu et al. (2018), which summarized physician workloads in China from 1998 to 2016. In 2015, there were 7.7 billion hospital visits, resulting in approximately 210 million inpatient admissions. We estimated the base incidence rate by dividing those patient numbers by the overall population in 2015. We projected the 2030 base incidence rate by increasing them by the same rates as the ones for mortality—1.333 for mainland China and 1.284 for Hong Kong.

The relative risks of both hospital admissions and outpatient visits for all ages were obtained from Cao et al. (2009) and Chen et al. (2010), respectively, which used the generalized linear Poisson models to generate the excess percentage risk for a 10 $\mu g/m^3$ increase of PM_{10} concentrations. The β coefficients were obtained from Equation 9, and the C1 and C0 used were modeled PM_{10} concentrations from 2030 BAU and 2030 ECA scenarios, respectively. RRs for both premature mortality and morbidity associated with a 10 $\mu g/m^3$ change in PM_{10} for studied health endpoints and their references can be found in Table 13.

[10] We used PM_{10} because our cited baseline incidence rate for morbidity was associated with PM_{10} concentrations (Cao et al., 2009). We did not estimate ECA-reduced morbidity related to O_3 emissions because no widely acceptable research has yet identified RRs that link O_3 emissions to hospital admissions or outpatient visits in the GPRD region.

Table 13. Relative risks of morbidity

Outcome and exposure metric	Relative Risks (95% CI)	Reference
Total outpatient visits and exposure to PM_{10}	1.0011 (0.9997, 1.0026)	Cao et al., 2009
Total hospital admission and exposure to PM_{10}	1.0018 (0.9985, 1.0052)	Chen et al., 2010

2.3.3 Health benefits monetization

We calculated the economic value of reduced mortality by applying the value of statistical life (VSL) method and quantified the economic benefits of reduced morbidity by applying the cost of illness (COI) method. The VSL is the estimated economic value of an average life, and the COI estimates both the costs of pharmaceuticals and hospitalization and the loss of income during sick leave due to illness. Lu, Yao, Fung, and Lin (2016) provided the VSLs and COIs for China from 2010 to 2013 based on the Consumer Price Index (CPI) in each year. We then projected to the 2015 level by linear interpolation and assumed that the VSL and CPI differences between 2030 and 2015 are negligible. The VSL used in this study is $1.15 million USD and the COIs for outpatient visit and hospital admission are $32.10 and $1,447.70, respectively. Because VSL is likely to grow over time as per capita income increases, our 2030 estimate for the monetized health benefits of a Chinese ECA could be considered conservative.

2.4 Cost analysis

To evaluate the cost effectiveness of a Chinese ECA in reducing SO_x, PM_{10} and NO_x emissions, we estimated the cost for ships to comply with a 200-nm ECA in 2030. The cost effectiveness of an ECA in 2030 is expressed as dollars per tonne of reduced emissions. The following assumptions for control measures were analyzed:

- ❏ All ships switched to MGO to comply with an ECA fuel sulfur limit of 1,000 ppm[11]
- ❏ All 4-stroke main engines built after 2025 are equipped with SCR to comply with Tier III NO_x regulations
- ❏ All 4-stroke auxiliary engines built after 2025 are equipped with SCR regardless of the technology applied to the main engine to comply with Tier III NO_x regulations
- ❏ All 2-stroke main engines built after 2025 are equipped with EGR to comply with Tier III NO_x regulations

The selection of technology was based on the availability and readiness of technology, as well as on analytical conclusions from previous ECA applications. In addition to cost-effectiveness, we calculated a cost-benefit ratio of an ECA policy for the GPRD region, which we compared against other land-based control measures. The total cost of ECA compliance should vary by region, as different ECAs cover different amounts of ship traffic. In this study, the total cost of ECA compliance for the GPRD region is a product of the cost-effectiveness per pollutant

[11] We did not consider scrubbers as a compliance option to meet the fuel sulfur requirement since China is planning to ban waste water discharge from open-loop scrubbers in its territorial waters (MSA, 2018). This will serve to discourage the use of scrubbers to comply with a future Chinese ECA. The official regulation can be found at http://www.xindemarinenews.com/uploads/soft/190105/285-1Z1051A610.pdf.

($/tonne) and the amount of ship emissions (tonnes) mitigated in a predefined region (see Section 3.4.2 in the main document for details).

2.4.1 Fuel-switching

The estimation of fuel-switching cost is straightforward (see Equation 12). Fuel consumption within the ECA in 2030 was estimated using the emissions projection model described in the previous section. The baseline 2030 fuel was assumed to be low-sulfur HFO (LSHFO), whereas the ECA-compliant fuel type is MGO (distillate fuel). Differences in the energy density of these fuels was corrected for by using assumptions outlined in Comer (2019).

$$C_{fuel\ switching} = FC_{distillate\ fuel} * P_{distillate\ fuel} - FC_{global\ fuel} * P_{global\ fuel} \quad (12)$$

Where:

$C_{fuel\ switching}$ = cost of fuel switching
$FC_{distillate\ fuel}$ = distillate fuel consumption within ECA, in tonnes
$P_{distillate\ fuel}$ = distillate fuel price, in $/tonne
$FC_{global\ fuel}$ = global marine fuel consumption within ECA, in tonnes
$P_{global\ fuel}$ = global marine fuel price, in $/tonne

The cost of fuel-switching is the price differential between ECA-compliant fuel (MGO) and global marine fuel (LSHFO). Mao and Rutherford (2018) used the World Bank's periodic projection of crude oil prices to estimate the 2025 prices for MGO and LSHFO for three generic (high, medium, and low) scenarios. We assumed that MGO and LSHFO prices track closely with that of the crude oil. Following the same methodology, we estimated the 2030 price for MGO and LSHFO (see Table 14). The price differential of the medium scenario (bold values) was used in the main analysis and those of the high and low scenarios were used for a sensitivity analysis. Additional details are provided in the Appendix to the main document.

Table 14. Fuel price estimates for 2030

Fuel type		2015 (2012 $ per tonne)	2020 (2012 $ per tonne)	2030 (2012 $ per tonne)		
				High	Medium	Low
Crude oil		382	454	1212	461	312
MGO		654	554	1481	***563***	381
LSHFO	High differential	-	-	1185	451	305
	Medium differential			1303	***496***	335
	Low differential			1422	541	366

2.4.2 Tier III NO_x control measures

In the North American ECA application, SCR was the only technology analyzed to comply with ECA NO_x regulations. In this study, we adopted the methodology detailed in a Danish Economic Impact Assessment study (Incentive Partners & Litehauz, 2012) (hereafter "the EIA study") that considered both SCR and EGR as compliance options. That recent study also was used to support the North Sea ECA application, and it likely better reflects recent technological developments and other developments that impact the economic viability of these technologies.

At the core of the EIA study was a cost function to estimate the capital and operational costs of SCR and EGR technologies on both 2-stroke and 4-stroke engines (see Table 12, adapted from Table 4-3 of the EIA study).

Table 15. NO_x control costs

Cost component	EGR (2-stroke)	SCR (4stroke)
Capital expenditure Y; 2012 $/kW (X = installed engine power, in MW)	-0.23X + 53.6	$0.03X^2$ - 2.07X + 65.1
Operational expenditure; 2012 $/MWh	2.85 (2.3-3.4)	8 (3.1–8.2)
SFOC; g/kWh	0.6	1.5 (1–2)

Note: When there is a range of values, the applied value reflects the arithmetic mean.

Capital cost (CAPEX) was calculated based on survey information from key manufacturers and expressed as a function of the engine's installed power. The range of CAPEX reflects the lower and upper limits of installed engine power used by the manufacturers surveyed. These ranges also were used in the sensitivity analysis, which is in the Appendix of the main report. Operational cost (OPEX) is directly related to the use of the technology. For SCR, this is mainly the cost of urea as a reagent to convert NO_x into nitrogen and water. For EGR, this is mainly the cost of running an internal scrubber with NaOH neutralization on the routed exhaust gas before mixing it with the incoming combustion air. Running the EGR system usually means a slight SFOC penalty because the process reduces combustion temperature and thus efficiency. The SFOC increase associated with SCR is due to the energy used to run the SCR reactor and the monitoring/control system, and its use for urea injection/dosing.

To capture the cost of Tier III NO_x control technology in 2030, the CAPEX must be amortized. We used the following equation to calculate the annualized CAPEX:

$$EAC = C_{initial} * \frac{r}{1-(1+r)^{-p}} \quad (13)$$

Where:

EAC = equivalent annual cost, in $/year
$C_{initial}$ = initial capital investment, in $
r = discount rate, or cost of investment
p = number of years for discounting, in this case, a ship's useful life

Equation 14 was used to calculate costs by ship class and capacity bin, with the following inputs and assumptions:

- ❑ Only ships built after 2025 will incur cost for NO_x Tier III control measures
- ❑ Ships that travel in non-China ECAs (e.g., the North American ECA, the North Sea ECA) split CAPEX among each ECA in proportion to the travel time within each. The split ratio can be found in Table 16
- ❑ The EIA study provided a range of OPEX values that are used in a sensitivity analysis detailed in the Appendix to the main document. The OPEX number used in this analysis was the suggested value used by the EIA study. These values are summarized in Table 15.

- ❑ CAPEX is expressed as an annuity in Equation 13. The discount rate was assumed to be 4%, as used in the EIA study. The period of discounting was assumed to be 25 years, the assumed useful life of a ship in this study.

$$C_{Tier\ III,k,l} = EAC_{k,l} * R\_ECA_{k,l} + OPEX_{k,l} \quad (14)$$

Where:

l	= ship capacity bin l
$C_{Tier\ III,k,l}$	= cost of Tier III NO_x compliance for ship class k and capacity bin l, in $
$EAC_{k,l}$	= equivalent annual capital cost of Tier III NO_x compliance for ship class k and capacity bin l, in $
$R\_ECA_{k,l}$	= ratio to split cost between the ECA under analysis and the rest of the ECAs
$OPEX_{k,l}$	= operational cost of Tier III NO_x compliance for ship class k and capacity bin l, in $

We allocated Tier III NO_x capital costs among the Chinese ECA and other ECAs based on the anticipated time a ship would spend in the Chinese ECA versus other ECAs around the world. We estimated a time ratio spent in existing versus a potential 200-nm Chinese ECA across different ship classes by sampling the 2015 OGV fleet. The ratios generated, shown in Table 16, range from 0.15 to 1.00; that is, for every 100 hours spent in all ECAs around the world, including the potential 200-nm Chinese ECA, ships would spend between 15 and 100 hours within the Chinese ECA.[12] If more ECAs are in place in 2030, then this ratio could be even lower, meaning less cost to China.

Table 16. China ECA ratio by ship class and capacity bin

Ship class	Capacity bin	Time ratio in China ECA
Container ship	1	1.00
	2	1.00
	3	1.00
	4	1.00
	5	1.00
	6	0.72
	7	1.00
	8	0.72
Bulk carrier	1	1.00
	2	1.00
	3	0.38
	4	0.39
	5	0.48
	6	1.00
General cargo ship	1	1.00
	2	1.00
	3	1.00
Chemical tanker	1	1.00
	2	1.00
	3	1.00
	4	0.15
Oil tanker	1	1.00

[12] Ships that never appeared in the potential Chinese ECA in 2015 were excluded from sampling.

	2	1.00
	3	1.00
	4	1.00
	5	0.08
	6	1.00
	7	1.00
	8	0.88
Liquified gas tanker	1	1.00
	2	0.69
	3	1.00
Cruise ship	2	1.00
	3	0.32
	4	0.68
	5	1.00
Roll-on/roll-off	1	1.00
	2	0.84
Refrigerated bulk	1	1.00
Vehicle	1	0.81
Tug boat	1	1.00
Fishing boat	1	1.00

The cost-effectiveness of the ECA in reducing NO_x emissions was then calculated by dividing the total cost by the total amount of emissions abated in the entire 200-nm national ECA.

References

Ackermann, I. J., Hass, H., Memmesheimer, M., Ebel, A., Binkowski, F. S., & Shankar, U. (1998). Modal aerosol dynamics model for Europe: Development and first applications. *Atmospheric Environment, 32*(17), 2981–2999. doi:10.1016/S1352-2310(98)00006-5

Boylan, J. W., & Russell, A. G. (2006). PM and light extinction model performance metrics, goals, and criteria for three-dimensional air quality models. *Atmospheric Environment*, 40(26), 4946–4959. doi:10.1016/j.atmosenv.2005.09.087

Burnett, R. T., Pope C. A., Ezzati, M., Olives, C., Lim, S. S., Mehta, S., … Cohen, A. (2014). An integrated risk function for estimating the global burden of disease attributable to ambient fine particulate matter exposure. *Environmental Health Perspectives*, 122(4), 397–403. doi:10.1289/ehp.1307049

Cai, S., Ma, Q., Wang, S., Zhao, B., Brauer, M., Cohen, A., ... Burnett, R. T. (2018). Impact of air pollution control policies on future $PM_{2.5}$ concentrations and their source contributions in China. *Journal of Environmental Management*, 227, 124–133. doi:10.1016/j.jenvman.2018.08.052

Cao, J., Li, W., Tan, J., Song, W., Xu, X., Jiang, C., … Kan, H. (2009). Association of ambient air pollution with hospital outpatient and emergency room visits in Shanghai,

China. *Science of The Total Environment*, 407(21), 5531–5536. doi:10.1016/j.scitotenv.2009.07.021

Center for International Earth Science Information Network—CIESIN—Columbia University. (2016). Gridded population of the world, version 4 (GPWv4): Administrative unit center points with population estimates. Palisades, NY: NASA Socioeconomic Data and Applications Center (SEDAC). doi:10.7927/H4F47M2C

Chang, J. C., & Hanna, S. R. (2004). Air quality model performance evaluation. *Meteorology and Atmospheric Physics*, 87(1–3). doi:10.1007/s00703-003-0070-7

Chen, C., E. Saikawa, B. Comer, X. Mao, and D. Rutherford, Ship Emission Impacts on Air Quality and Human Health in the Pearl River Delta (PRD) region, China in 2015, with Projections to 2030, GeoHealth, https://doi.org/10.1029/2019GH000183, in press.

Chen, R., Chu, C., Tan, J., Cao, J., Song, W., Xu, X., … Kan, H. (2010). Ambient air pollution and hospital admission in Shanghai, China. *Journal of Hazardous Materials*, 181(1–3), 234–240. doi:10.1016/j.jhazmat.2010.05.002

Chen, D., Zhao, N., Lang, J., Zhou, Y., Wang, X., Li, Y., … Guo, X. (2018). Contribution of ship emissions to the concentration of $PM_{2.5}$: A comprehensive study using AIS data and WRF/Chem model in Bohai Rim Region, China. *Science of The Total Environment*, 610–611, 1476–1486. doi:10.1016/j.scitotenv.2017.07.255

China Maritime Safety Administration. (2018). *Notice for implementing the Domestic Emission Control Areas.* Retrieved from Xinde Marine News website, http://www.xindemarinenews.com/uploads/soft/190105/285-1Z1051A610.pdf

Comer, B., Olmer, N., Mao, X., Roy, B., & Rutherford, D. (2017). *Black carbon emissions and fuel use in global shipping, 2015.* Retrieved from the International Council on Clean Transportation, https://theicct.org/publications/black-carbon-emissions-global-shipping-2015

Comer, B. (2019). *Transitioning away from heavy fuel oil in Arctic shipping*. Retrieved from the International Council on Clean Transportation, https://www.theicct.org/sites/default/files/publications/Transitioning_from_hfo_Arctic_20190218.pdf

Emmons, L. K., Walters, S., Hess, P. G., Lamarque, J.-F., Pfister, G. G., Fillmore, D., … Kloster, S. (2010). Description and evaluation of the model for ozone and related chemical tracers, version 4 (MOZART-4). *Geoscientific Model Development*, 3(1), 43–67. doi:10.5194/gmd-3-43-2010

Fu, Y., Schwebel, D. C., & Hu, G. (2018). Physicians' workloads in China: 1998–2016. *International Journal of Environmental Research and Public Health*, 15(8), 1649. doi:10.3390/ijerph15081649

Grell, G. A., Peckham, S. E., Schmitz, R., McKeen, S. A., Frost, G., Skamarock, W. C., & Eder, B. (2005). Fully coupled "online" chemistry within the WRF model. *Atmospheric Environment*, 39, 6957–6975. doi:10.1016/j.atmosenv.2005.04.027

Gong, S. L. (2003). A parameterization of sea-salt aerosol source function for sub- and super-micron particles, *Global Biogeochemical Cycles*, 17(4), 1097. doi:10.1029/2003GB002079

Guenther, A. B., Jiang, X., Heald, C. L., Sakulyanontvittaya, T., Duhl, T., Emmons, L. K., & Wang, X. (2012). The model of emissions of gases and aerosols from nature version 2.1 (MEGAN2.1): An extended and updated framework for modeling biogenic emissions. Geoscientific Model Development, 5(6), 1471–1492. doi:10.5194/gmd-5-1471-2012

Hon, G., & Wang H. (2011). *The energy efficiency design index (EEDI) for new ships*. Retrieved from the International Council on Clean Transportation, https://www.theicct.org/publications/energy-efficiency-design-index-eedi-new-ships

Incentive Partners & Litehauz. (2012). *Economic impact assessment of a NO_x emission control area in the North Sea.* Retrieved from https://www2.mst.dk/Udgiv/publications/2012/06/978-87-92903-20-4.pdf

International Maritime Organization. (2016). Module 2 – Ship energy efficiency regulations and related guidelines. In Z. Bazari (Ed.), *IMO train the trainer (TTT) course on energy efficient ship operation*. Retrieved from http://www.imo.org/en/OurWork/Environment/PollutionPrevention/AirPollution/Documents/Air%20pollution/M2%20EE%20regulations%20and%20guidelines%20final.pdf

Janssens-Maenhout, G., Crippa, M., Guizzardi, D., Dentener, F., Muntean, M., Pouliot, … Li, M. (2015). HTAP_v2.2: A mosaic of regional and global emission grid maps for 2008 and 2010 to study hemispheric transport of air pollution, *Atmospheric Chemistry and Physics*, 15, 11411–11432, doi:10.5194/acp-15-11411-2015

Jerrett, M., Burnett, R. T., Pope, C. A., Ito, K., Thurston, G., Krewski, D., … Thun, M. (2009). Long-term ozone exposure and mortality. *New England Journal of Medicine, 360*(11), 1085–1095. doi:10.1056/NEJMoa0803894

Kurokawa, J., Ohara, T., Morikawa, T., Hanayama, S., Janssens-Maenhout, G., Fukui, T., … Akimoto, H. (2013). Emissions of air pollutants and greenhouse gases over Asian regions during 2000–2008: Regional emission inventory in Asia (REAS) version 2, *Atmospheric Chemistry and Physics*, 13, 11019–11058. doi:10.5194/acp-13-11019-2013

Lin, H., Liu, T., Xiao, J., Zeng, W., Li, X., Guo, L., … Ma, W. (2016). Mortality burden of ambient fine particulate air pollution in six Chinese cities: Results from the Pearl River Delta study, *Environment International*, 96, 91–97. doi:10.1016/j.envint.2016.09.007

Liu, H., Jin, X., Wu, L., Wang, X., Fu, M., Lv, Z., … He, K. (2018). The impact of marine shipping and its DECA control on air quality in the Pearl River Delta, China. *Science of The Total Environment*, 625, 1476–1485. doi:10.1016/j.scitotenv.2018.01.033

Lu, X., Yao, T., Fung, J. C. H., & Lin, C. (2016). Estimation of health and economic costs of air pollution over the Pearl River Delta region in China. *Science of the Total Environment*, 566–567, 134–143. doi:10.1016/j.scitotenv.2016.05.060

Ma, Q., Cai, S. Y., Wang, S., Zhao, B., Martin, R. V., Brauer, M., … Burnett, R. T. (2017). Impacts of coal burning on ambient $PM_{2.5}$ pollution in China. *Atmospheric Chemistry and Physics*, 17(7), 4477–4491. doi:10.5194/acp-17-4477-2017

Mao, X., & Rutherford, D. (2018). *Delineating a Chinese emission control area: The potential impact of ship rerouting on emissions*. Retrieved from the International Council on Clean Transportation, https://www.theicct.org/publications/delineating-chinese-emission-control-area

Morris, R. E., B. Koo, B. Wang, G. Stella, D. McNally, C. Loomis, C. J. Chien, and G. Tonnesen (2007), Technical support document for VISTAS emissions and air quality modeling to support regional haze State Implementation Plans, Tech. Rep., VISTAS Technical Coordinator, http://pah.cert.ucr.edu/vistas/vistas2/reports/TSD/

National Centers for Environmental Prediction. (n.d.). NCEP FNL operational model global tropospheric analyses, continuing from July 1999. doi:10.5065/D6M043C6

Olmer, N., Comer, B., Roy, B., Mao, X., & Rutherford, D. (2017). *Greenhouse gas emissions from global shipping, 2013–2015*. Retrieved from the International Council on Clean Transportation, http://theicct.org/sites/default/files/publications/Global-shipping-GHG-emissions-2013-2015_ICCT-Report_17102017_vF.pdf

Riahi, K., Rao, S., Krey, V., Cho, C., Chirkov, V., Fischer, G. … Rafaj, P. (2011). RCP 8.5—A scenario of comparatively high greenhouse gas emissions. *Climatic Change, 109*(1-2), 33. doi:10.1007/s10584-011-0149-y

Schell, B., Ackermann, I. J., Hass, H., Binkowski, F. S., & Ebel, A. (2001). Modeling the formation of secondary organic aerosol within a comprehensive air quality model system. *Journal of Geophysical Research: Atmospheres*, 106, 28275–28293. Retrieved from https://agupubs.onlinelibrary.wiley.com/doi/pdf/10.1029/2001JD000384

Shanghai International Shipping Institute. (2015). *China shipping development outlook 2030*. Retrieved from http://en.sisi-smu.org/index.php?c=article&id=13534

Shaw, W. J., Allwine, K. J., Fritz, B. G., Rutz, F. C., Rishel, J. P., & Chapman, E. G. (2008). An evaluation of the wind erosion module in DUSTRAN, *Atmospheric Environment*, 42(8), 1907–1921. doi:10.1016/j.atmosenv.2007.11.022

Smith, T. W. P., Jalkanen, J. P., Anderson, B. A., Corbett, J. J., Faber, J., Hanayama, S., ... Pandey, A. (2015). *Third IMO greenhouse gas study 2014*. Retrieved from the International Maritime Organization, http://www.imo.org/en/OurWork/Environment/PollutionPrevention/AirPollution/Documents/Third%20Greenhouse%20Gas%20Study/GHG3%20Executive%20Summary%20and%20Report.pdf

Stockwell, W. R., Middleton, P., Chang, J. S., & Tang, X. (1990). The second generation regional acid deposition model chemical mechanism for regional air quality modeling. *Journal of Geophysical Research: Atmospheres*, 95, 16343–16367, doi:10.1029/JD095iD10p16343

Tao, Y., Huang, W., Huang, X., Zhong, L., Lu, S.-E., Li, Y., … Zhu, T. (2012). Estimated acute effects of ambient ozone and nitrogen dioxide on mortality in the Pearl River Delta of Southern China. *Environmental Health Perspectives*, 120(3), 393–398. doi:10.1289/ehp.1103715

UN Department of Economic and Social Affairs. (n.d.). *World population prospects 2019*. Accessed November 26, 2018, https://population.un.org/wpp/DataQuery/

United Nations, Department of Economic and Social Affairs, Population Division (2017). World Population Prospects: The 2017 Revision, Methodology of the United Nations Population Estimates and Projections, Working Paper No. ESA/P/WP.250. New York: United Nations.

United Nations Conference on Trade and Development. (n.d.) Review of maritime transport (series), retrieved from https://unctad.org/en/Pages/Publications/Review-of-Maritime-Transport-(Series).aspx

U.S. Environmental Protection Agency. (2009). *Proposal to designate an emission control area for nitrogen oxides, sulfur oxides and particulate matter* (Technical support document). Retrieved from https://19january2017snapshot.epa.gov/sites/production/files/2016-09/documents/420r09007.pdf

Viana, M., Hammingh, P., Colette, A., Querol, X., Degraeuwe, B., Vlieger, I. de, & van Aardenne, J. (2014). Impact of maritime transport emissions on coastal air quality in Europe. *Atmospheric Environment*, 90, 96–105. doi:10.1016/j.atmosenv.2014.03.046

Wang, H., & Lutsey, N. (2013). *Long-term potential for increased shipping efficiency through the adoption of industry-leading practices*. Retrieved from the International

Council on Clean Transportation, https://www.theicct.org/publications/long-term-potential-increased-shipping-efficiency

Wild, O., Zhu, X., & Prather, M. (2000). Fast-J: Accurate simulation of in- and below-cloud photolysis in tropospheric chemical models. *Journal of Atmospheric Chemistry*, 37, 245–282. doi:10.1023/A:1006415919030